Journal of ELECTRICAL ENGINEERING, VOL 72(2021), NO4, 229–239

sciendo

PAPERS

Frequency domain despeckling technique for medical ultrasound images

Jawad F. Al-Asad[1*], Hiren K. Mewada[1], Adil H. Khan[1], Nidal Abu-Libdeh[2], Jamal F. Nayfeh[3]

This work proposes a novel frequency domain despeckling technique pertaining to the enhancement of the quality of medical ultrasound images. The results of the proposed method have been validated in comparison to both the time-domain and the frequency-domain projections of the schur decomposition as well as with several other benchmark schemes such as frost, lee, probabilistic non-local means (PNLM) and total variation filtering (TVF). The proposed algorithm has shown significant improvements in edge detection and signal to noise ratio (SNR) levels when compared with the performance of the other techniques. Both real and simulated medical ultrasound images have been used to evaluate the numerical and visual effects of each algorithm used in this work.

K e y w o r d s: despeckling, schur decomposition, ultrasound image, covariance matrix, frequency domain, orthonormal vectors

1 Introduction

The monitoring and diagnosis of diseases in the human body are immensely dependent on medical imaging. Through various available imaging technologies, the inside of a human subject can be better examined and more accurate disease diagnosis and/or prognoses prescribed by healthcare professionals. Ultrasound is one of the essential and conventional medical imaging modalities that work on the principle of acoustic energy. Unlike Xrays, CT, and MRI images, ultrasound is a non-invasive real-time imaging paradigm [1]. The ultrasound imaging is a non-ionized method that tends to have less adverse effects on the human body. Ultrasound imaging is therefore usually preferred over other medical imaging modalities if it provides reasonable details for analysis.

The major disadvantage carried by ultrasound images is the inclusion of multiplicative noise, also known as speckle noise, during the process of image acquisition [2]. A high amount of speckle-noise is accumulated in ultrasound images due to a complex phenomenon of destructive and constructive interference of echoes from various neighboring tissue parts in the body. The granular effect generated due to the presence of speckle noise degrades overall the image quality and resolution of tiny details in the ultrasound images, which carries immense importance for a correct medical diagnosis [3]. Speckle noise is highly dependent on various parameters, such as the specific image type and structure of tissues or cells of the human body. Therefore, it is a tedious task to model speckle-noise efficiently. In light of addressing the critical issue of speckle-noise removal from ultrasound images, various research studies have been performed in the last two decades to design despeckling filters that can aid in the enhancement of the quality of the ultrasound images[4].

2 Recent work

Proposed despeckling algorithms can be categorized into spatial domain and frequency domain filters in a broad sense. Spatial domain methods usually rely on local statistics that characterize the information of restored images. Such methods include Frost [5], Kuan [6], and Lee [7] filters. The main drawback of these traditional methods is their poor performance in edge detection. Most successful among these are the diffusion-based [8] and bilateral filtering methods [9]. These methods preserve the edge information during the despeckling process due to sensitive diffusion along the edges. Still, these methods distort the correlation of neighboring pixels, and in the performance of dense noise, the despeckling efficiency decreases drastically. In the frequency domain analysis, methods based on wavelet decomposition are commonly used where speckle noise is converted into additive, and then removed through wavelet processing. Such noise filtering methods of ultrasound images are proposed in [3] and modifications are presented in [10] and [11]. In wavelet-based methods, the main disadvantage is the inclusion of artifacts in the image by the mother wavelet, which affects the image quality [12].

The Group of techniques based on non-local methods was used in the past to address the problem of local de-

Prince Mohammad Bin Fahd University, Kohbar, Kingdome of Saudi Arabia, 11952. [1] Electrical Engineering Department, [2] Department of Mathematics & Natural Sciences, [3] Mechanical Engineering Department, Correspondence: *jalasad@pmu.edu.sa

DOI:https://doi.org/10.2478/jee-2021-0032, Print (till 2015) ISSN 1335-3632, On-line ISSN 1339-309X

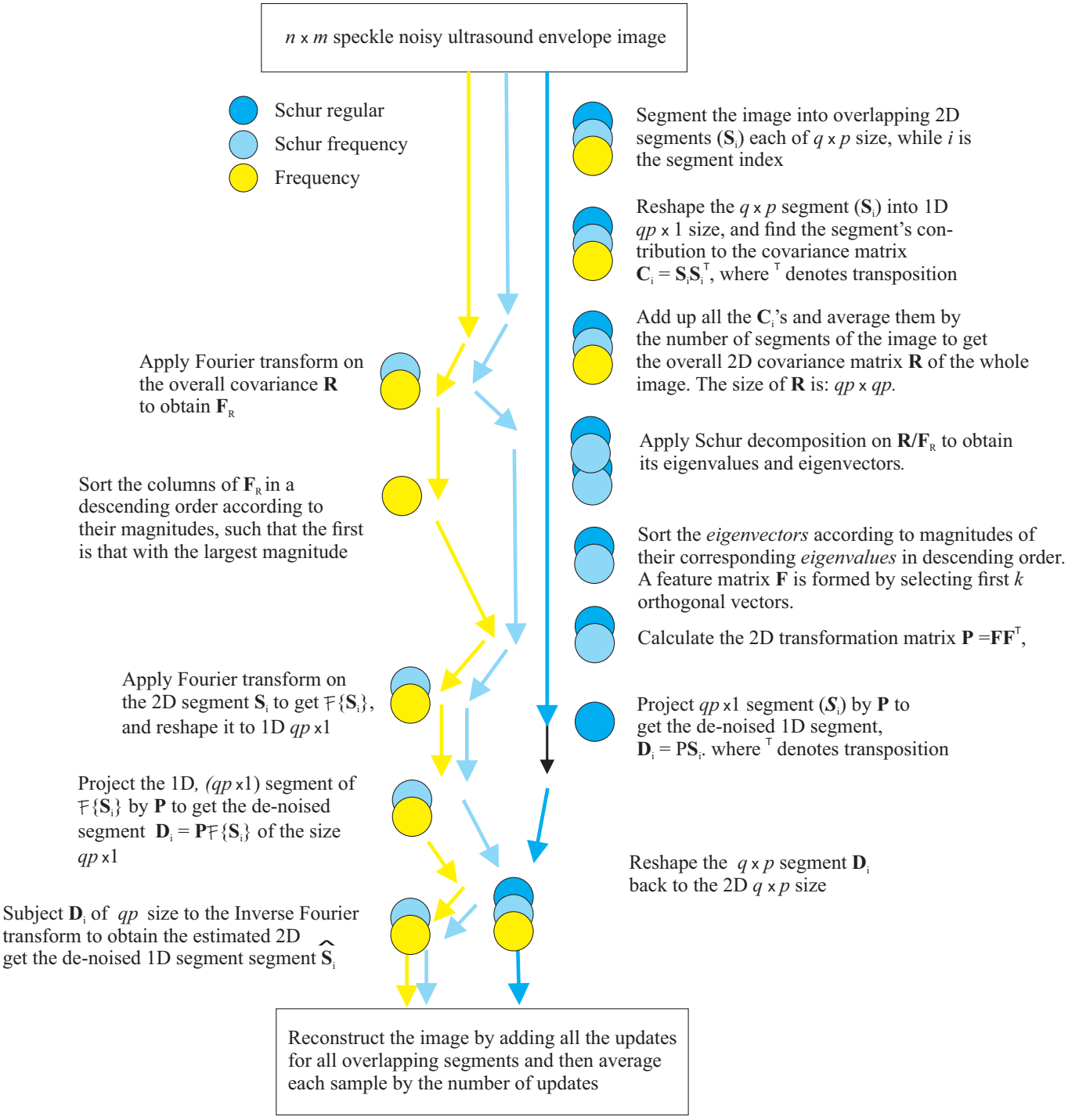

Fig. 1. Proposed frequency and Schur frequency despeckling algorithms compared to Schur regular

pendence. Such methods exploit the redundancy property between similar patches to minimize the effect of speckle-noise [13]. The problem with such approaches is the selection of the starting patch, that could have significant impact on despeckling performance, especially in the presence of grinding noise. This issue is addressed in [14], where a guidance image is used to select the starting patch. Another solution is provided in [15], where statistical properties are used with local and non-local attributes to choose the starting patch. Research has been done on the collaboration of block matching and non-local means, for example, in [16] Fisher Tippett the distribution is used for the calculation of patch distance to match them. Sometimes patches are applied as a square window to improve overall performance in non-local mean methods. Similar to patches, windows are used to recover pixels through the weighted average of the window. In [17] better despeckling results were obtained in which the weight

function of a non-local mean filter is replaced with probabilistic weights to reflect more similarity between two noisy patches.

In recent years, the use of projection-based methods in speckle removing increased as compared to conventional filters. In these methods, a global covariance matrix is secured by eigenvectors of overlapping blocks, and then the projection is used to clean the speckle noise. The performance of such approaches depends on the eigenvector decomposition and selection [18]. In [19], Schur decomposition is proposed for eigenvalue decomposition, and initial vectors were selected to minimize the effect of speckle noise. Frequency domain analysis is incorporated with Schur decomposition in [2], which secures much better results due to the analysis in the frequency domain. The drawback of these methods is the complexity of the algorithm. This issue is addressed using orthogonal decomposition in the frequency domain [20]. In [21], super-pixel is used with bilateral filtering where object boundaries are processed by incorporating local structure to reserve edge details and the resolution of recovered image. In [22], besides the mean value of pixels in the window, the mean of pixels surrounded by the window is also used. They propose criteria based on the standard deviation to select the pixels in the window's vicinity. The main advantage of this technique is the reduction of over smoothing, which is caused by the uniform averages.

3 Ultrasound signal model and image quality parameters

In order to create a simplified computational model for ultrasound images, the adverse effects of different types of noise are considered. The significant source of impairment in ultrasound images is speckle noise whereas and not the additive white Gaussian noise (AWGN). Therefore, the contribution of the additive part of noise is negligible and as such can be safely discarded for simplicity purposes. In [23], a noisy image model for ultrasound images has been explained. This study also develops a simplified technique by only incorporating the speckle noise

$$I(n,m) = J(n,m) + K(n,m), \tag{1}$$

The image $\boldsymbol{I}(n,m)$ is assumed to be observed before application of any pre-processing technique such as log-compression or non-linear amplification [23]. The performance assessment of despeckling algorithms is performed by analyzing both numerical and visual outcomes. For numerical evaluation, parameters such as (resolution), β (edge detection), CNR (contrast to noise ratio), SNR (signal to noise ratio), $PSNR$ (peak-signal to noise ratio) and $FSIM$ (feature similarity index) are utilized. The lower value of α and β being closer to 1 are indicators of better image resolution and preserving edge details, respectively. CR, SNR, and $PSNR$ represent the ratio of contrast, signal and peak-signal with respect to the speckle noisy component in the ultrasound image and are regarded as significant performance evaluation parameters. The value of $FSIM$ is normalized in the range [0,1], and a higher value denotes the better quality of the despeckled image.

4 Proposed algorithm in frequency domain

Assume that an ultrasound image with dimensions $n \times m$ is contaminated with speckles. The flowchart presented in Fig. 1 shows the various steps of the proposed Frequency domain despeckling technique, indicated by the white circle, along with the proposed Schur-frequency despeckling technique, indicated by the gray circle and the Schur regular despeckling technique, indicated by the dark circle. The proposed frequency and Schur frequency algorithms tend to eliminate the speckle noise by using subspace signal projections in the frequency domain. In contrast, the Schur regular algorithm tends to reduce the speckles in the spatial domain.

Initially, image $\boldsymbol{I}(n,m)$ is divided into a number of segments each of q-rows and p-columns. Let $\boldsymbol{S}_i$ be the i-th segment in the image plane. The total number of segments w can be calculated as

$$w = \frac{nm}{qp}. \tag{2}$$

Then covariance matrix of a pair of elements in the each segment is

$$\boldsymbol{C}_i = \begin{bmatrix} \operatorname{cov}(\boldsymbol{S}_{i1}, \boldsymbol{S}_{i1}) & \operatorname{cov}(\boldsymbol{S}_{i1}, \boldsymbol{S}_{i2}) & \cdots & \operatorname{cov}(\boldsymbol{S}_{i1}, \boldsymbol{S}_{in}) \\ \operatorname{cov}(\boldsymbol{S}_{i2}, \boldsymbol{S}_{i1}) & \operatorname{cov}(\boldsymbol{S}_{i2}, \boldsymbol{S}_{i2}) & \cdots & \operatorname{cov}(\boldsymbol{S}_{i2}, \boldsymbol{S}_{in}) \\ \vdots & \vdots & \ddots & \vdots \\ \operatorname{cov}(\boldsymbol{S}_{in}, \boldsymbol{S}_{i1}) & \operatorname{cov}(\boldsymbol{S}_{in}, \boldsymbol{S}_{i2}) & \cdots & \operatorname{cov}(\boldsymbol{S}_{in}, \boldsymbol{S}_{in}) \end{bmatrix}$$

where $t = qp$ and

$$\begin{aligned} &\operatorname{cov}(\boldsymbol{S}_{ij}, \boldsymbol{S}_{ik}) = \\ &= E\left[(S_{ij} - E[(S_{ij}])(S_{ik} - E[(S_{ik}])\right] = \\ &= E[S_{ij}S_{ik}] - E[S_{ij}]E[S_{ik}] \\ &\text{for } j,k = 1,2,\ldots w \end{aligned}$$

This covariance matrix de-correlates the pixel values in each segment of the image. Then the average of covariance matrix is calculated as

$$\boldsymbol{R} = \frac{1}{w}\sum_{i=1}^{w} \boldsymbol{C}_i. \tag{3}$$

The spectral methodology is simple and computationally fast. In addition, the eigenvalue decomposition of the matrix in the frequency domain allows analysis of the contributing factor separately. Eigenvalues computation in the frequency domain ensures smooth transition across the block and allows frequency-dependent vector decomposition. Therefore, the covariance matrix is transformed

Table 1. Despeckling parameters and computation cost

Method	Parameters	Complexity for N pixels
Frequency	Block size: 8×8, Vectors: {2, 4}	$O(N\log N)$
Schur-frequency	Block size: 8×8, Vectors: {2, 4}	$O(N^3)$
Schur-regular	Block size: 8×8, Vectors: {2, 4}	$O(N^3)$
Frost	Window size =	$O(N^2k)$ k : number of iterations
Lee	Window size: 3×3, Iterations = 3	$O(N^2k)$ k : number of iterations
PNLM	Patch size-half = 1, Search-size-half = 3 Correction Parameter = 1	$O(N^2h^2)$ h : window size
TVF	$\lambda = 30$, Number of iterations = 20	$O(Nk)$ k: number of iterations

into the frequency domain and the Schur decomposition that supports vector decomposition is used to obtain the eigenvalues thus ensuring better perceptual quality. This decomposition scheme at different frequencies is adopted instead of using the entire frequency spectrum of the image plane. The elements of complex-valued matrix $\boldsymbol{F}_R$ can be expressed as

$$F_R(u,v) = \sum_{x=0}^{t-1}\sum_{y=0}^{t-1} \boldsymbol{R}(x,y) e^{-j2\pi\left(\frac{ux}{t}+\frac{vy}{t}\right)}. \quad (4)$$

The Schur decomposition offers the advantages of numerical stability, computational efficiency and better reliability. The Schur decomposition can be expressed as

$$\boldsymbol{F}_R = \boldsymbol{U}\boldsymbol{A}\boldsymbol{U}^{\mathrm{H}}, \quad (5)$$

where $\boldsymbol{U}$ is an orthogonal matrix, $\boldsymbol{A}$ is an upper-triangular matrix, and "H" means Hermitian transpose. The diagonal elements of $\boldsymbol{A}$ are the Schur values and the columns of the orthogonal matrix $\boldsymbol{U}$ defines the Schur vectors. Then, a feature matrix $\boldsymbol{F}$ is generated by selecting the first K Schur vectors corresponding to the K largest Schur values. A transformation matrix $\boldsymbol{P}$ froms the feature matrix $\boldsymbol{F}$ is calculated as

$$\boldsymbol{P} = \boldsymbol{F}\boldsymbol{F}^{\top}, \quad (6)$$

which is used to denoise the particular segment for which it has been obtained.

To remove the noise from the image segment, the segment is transformed into the frequency domain. If the Fourier transform of the segment is represented as $\mathcal{F}\{\boldsymbol{S}_i\}$, then the projection of the vector obtained from $\mathcal{F}\{\boldsymbol{S}_i\}$ can be calculated as $\boldsymbol{D}_i = \boldsymbol{P}\mathcal{F}\{\boldsymbol{S}_i\}$. To get the denoised segment back, a vector $\boldsymbol{D}_i$ is reshaped to a matrix, and the inverse Fourier transform is calculated as follows

$$\hat{\boldsymbol{S}}_i(x,y) = \frac{1}{qp}\sum_{x=0}^{q-1}\sum_{y=0}^{p-1} \boldsymbol{D}_i(u,v) e^{j2\pi\left(\frac{ux}{q}+\frac{vy}{p}\right)}. \quad (7)$$

This process is repeated for all overlapping segments of an image. This Schur-Frequency despeckling procedure is followed in [19]. The same procedure is also followed for Schur regular despeckling but without incorporating the frequency domain. The same procedure is also used for Frequency despeckling, but this time, without incorporating Schur decomposition.

The objectives of transforming the covariance matrix to the frequency domain and using the frequency vectors to form a feature matrix and thereafter a projection matrix are three folds: to suppress speckle noise to further reduce the computational complexity of the despeckling technique; and to maintain an efficient despeckling performance The computational procedure is fully detailed in Fig. 1.

5 Results and discussion

5.1 Simulated ultrasound image

A noise-free ultrasound image of the abdomen region is created by performing simulation using the Field II program [24], as depicted in Fig. 2(a). Linear scanning has been applied to the noise-free ultrasound image, and the size of the image is adjusted to 256×256. The speckle noise is incorporated into the noise-free image using (1), and the result is depicted in Fig. 2(b). The proposed and benchmark despeckling techniques are applied to the noisy image in Fig. 2-(b). A comparison is made with the noise-free image Fig. 2(a) to assess the despeckling ability of each scheme.

The parameters are being set to produce the best visual results for both proposed and benchmark schemes as listed in Tab. 1. The proposed Frequency and Schur-frequency schemes are implemented in an overlapping design with each block having a size of 8×8. Two and four orthonormal vectors where found to produce satisfying results. The proposed techniques are compared with benchmark algorithms such as Frost [5], Lee [7], PNLM [15], TVF [25] and Schur regular [19]. The despeckled images with four vectors are depicted in Fig. 2(c) through (i) and the corresponding numerical outcomes are listed in Tab. 2 after averaging results of 50 independent trials. The proposed approaches outperformed all benchmarking algorithms with reference to SNR, $PSNR$, β and $FSIM$ while maintaining a reasonable performance in

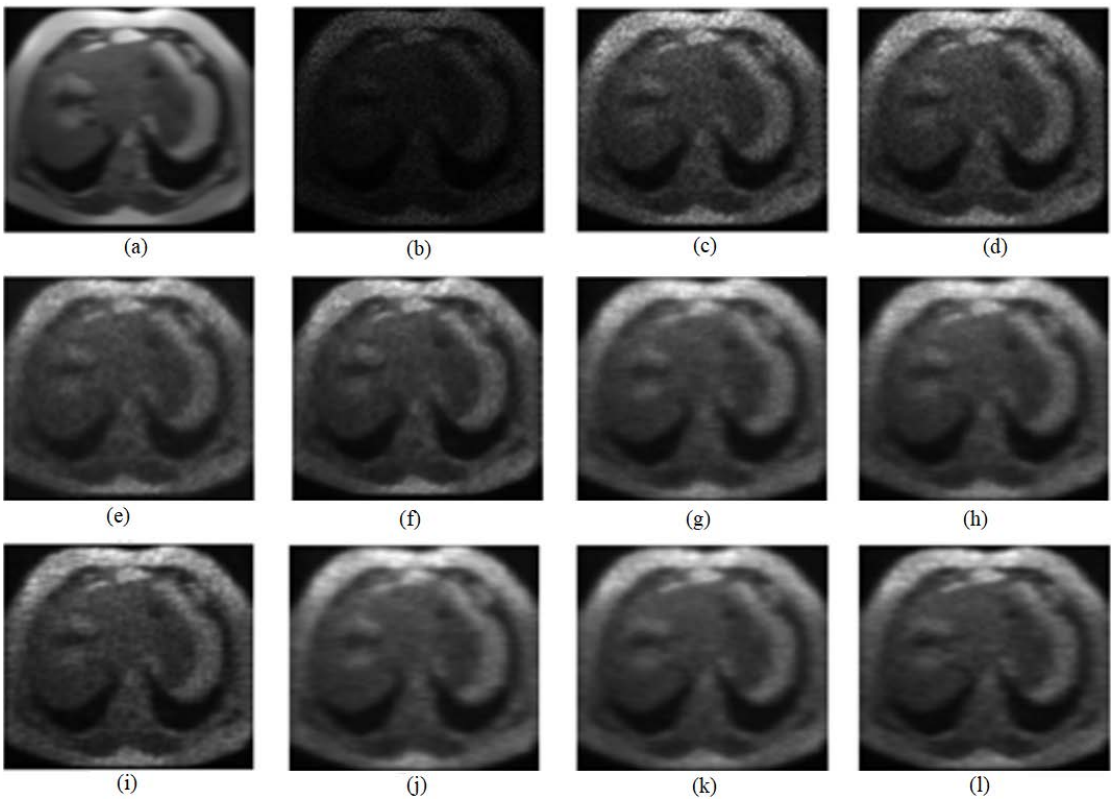

Fig. 2. Simulated visual results; noise free (a) – speckle noisy, (b) – Frost, (c) – Lee (d) – PNLM, (e) – TVF, (f) – frequency $8\times 8, 4$,(g) – Schur-frequency $8\times 8, 4$, (h) – Schur-regular $8\times 8, 4$, (i) – frequency 8×8.2, (j) – Schur-frequency $8\times 8, 2$, (k) – Schur-regular $8\times 8, 2$ (1)

Table 2. Comparison of the proposed approach with state-of-art filters

	Frequency	Schur-frequency	Schur-regular				
Block	8×8	8×8	8×8	Frost	Lee	PNLM	TVF
Vectors	4	4	4				
α	0.0809	0.0834	0.0810	0.0667	0.0799	0.0390	0.0851
β	0.2541	0.2639	0.2305	0.1757	0.1804	0.1718	0.2706
CNR	0.2331	0.2339	0.2067	0.2226	0.2163	0.2454	0.1792
SNR	18.4030	18.7185	15.9756	14.0325	15.4843	16.1730	15.9170
PSNR	26.1197	26.3660	24.4960	22.7154	23.8975	23.7575	24.2891
FSIM	0.9143	0.9146	0.8957	0.8501	0.8728	0.8575	0.9141

terms of α and CR. Another impressive feature of applying the proposed computational scheme is its superior performance in terms of edge preservation (β). Usually, better despeckling is secured at the cost of a decrease in sharpness. The benchmark schemes; Frost, Lee, PNLM and TVF have generally showed better performance in terms of resolution (α) but that is at the cost of poor despeckling as per visual and numerical outcomes of Fig. 2 and Tab. 2. A block size of 8×8 with one and two orthonormal vectors and a block size of 4×4 with 2 vectors are also investigated and their numerical results as an average of 50 independent trials are listed in Table 3. It was found that using a dyadic block size less than 8×8 will leave the image despeckled inefficiently. This conclusion can be reached by looking at the SNR and $PSNR$ parameters in Table 3 for the 4×4 block size and comparing them with those of 8×8 block size. On the other hand, using a block size of 8×8 with one vector will over smooth the despeckled image. This result is clearly realized by looking at the numerical results for block size 8×8 with one vector in Table 3 and comparing them with the corresponding ones in Tab. 2 for block size 8×8 with four vectors. Block size of 8×8 with one vector has caused poor edge detection and resulted in a blurry image as indicated by the increase of the resolution parameter α. By investigating Tab. 2 and Tab. 3 for block size proposed schemes mainly in CR. Further, for block size 8x8 with four and two orthonormal vectors respectively, we can notice that the proposed methods (Frequency and Schur Frequency) have clearly outperformed Schur Regular when the num-

Table 3. Simulated numerical results analysis using parameter variation

	Frequency			Schur-frequency			Schur-regular		
Block	4×4	8×8	8×8	4×4	8×8	8×8	4×4 4	8×8	8×8
Vectors	2	1	2	2	1	2	2	1	2
α	0.0542	0.1031	0.0968	0.0553	0.1031	0.0969	0.0523	0.1031	0.0928
β	0.1837	0.1676	0.2975	0.1818	0.1696	0.3020	0.1741	0.1674	0.2813
CNR	0.2304	0.2164	0.2147	0.2324	0.2155	0.2152	0.2291	0.2184	0.1841
SNR	13.2534	18.1667	20.1968	13.4043	18.1290	20.4012	12.4835	17.9838	20.5857
PSNR	22.0813	26.4122	27.6068	22.2195	26.4288	27.8330	21.3849	26.3517	27.2533
FSIM	0.8408	0.9213	0.9304	0.8455	0.9219	0.9319	0.8124	0.9227	0.9347

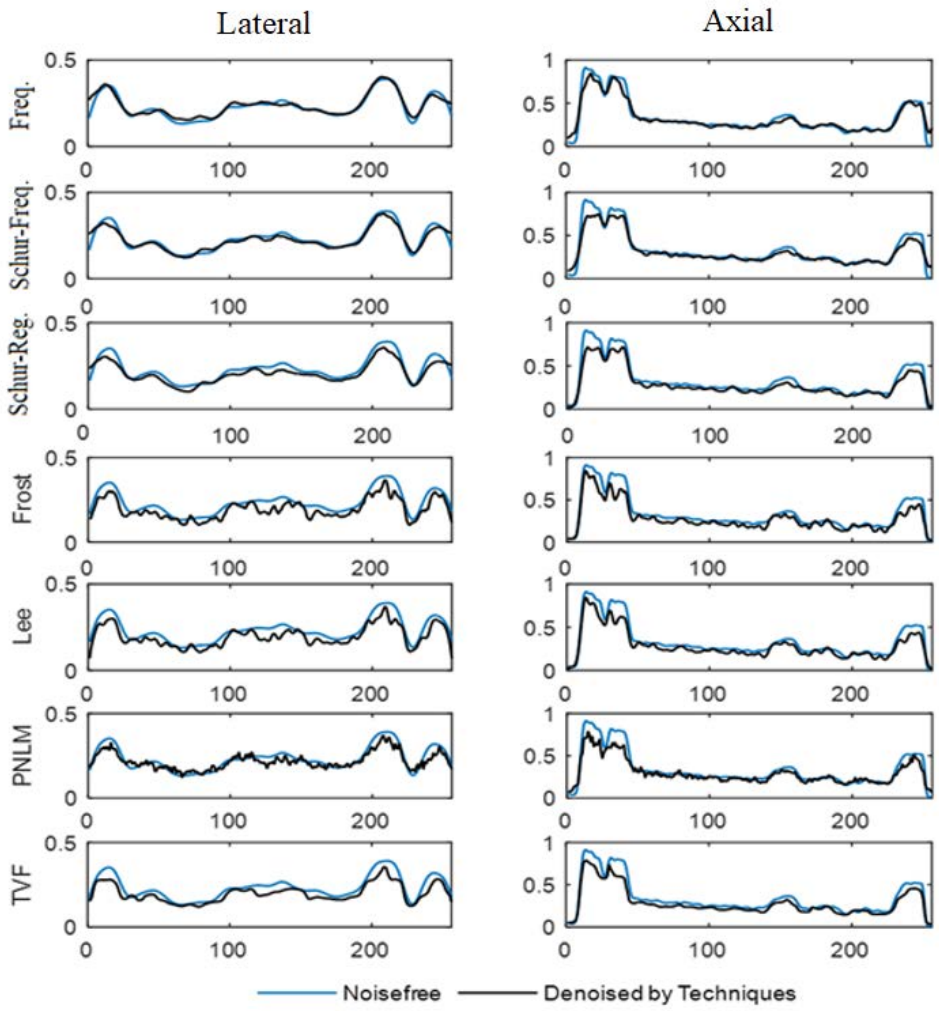

Fig. 3. Simulated image profiles analysis

ber of vectors are four. When the number of vectors are two, the Schur Regular has showed noticeable improvement in performance but it is still lagging Frequency and Schur-Frequency proposed schemes mainly in CR.

Based on the aforementioned discussion of the results, it is quite obvious that despeckling the image in the frequency domain yields better estimation of the original image than despeckling it in the time or spatial domain. Tab. 2 and Tab. 3 also show that the proposed Frequency and Schur frequency schemes are almost equivalent in the despeckling performance. That is a projection matrix formed from the fourier transformed covariance matrix is as efficient as the projection matrix formed from the Schur decomposed fourier transformed covariance matrix.

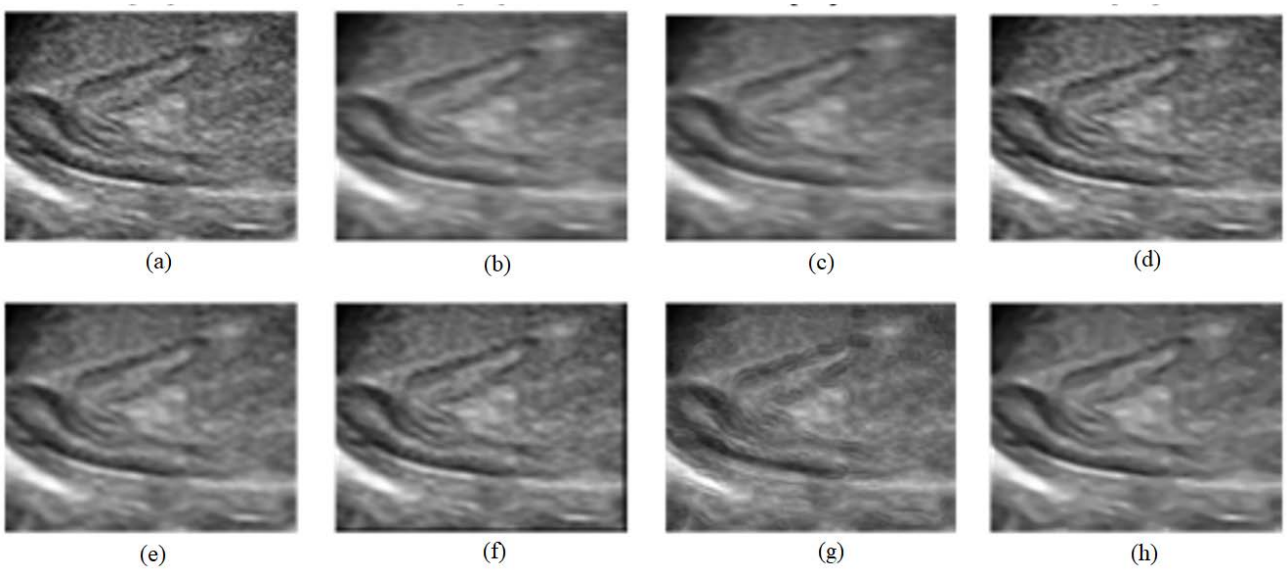

Fig. 4. Real abdomen visual results: (a) – speckle noisy, (b) – frequency 8×8, 4 (b) – Schur-frequency

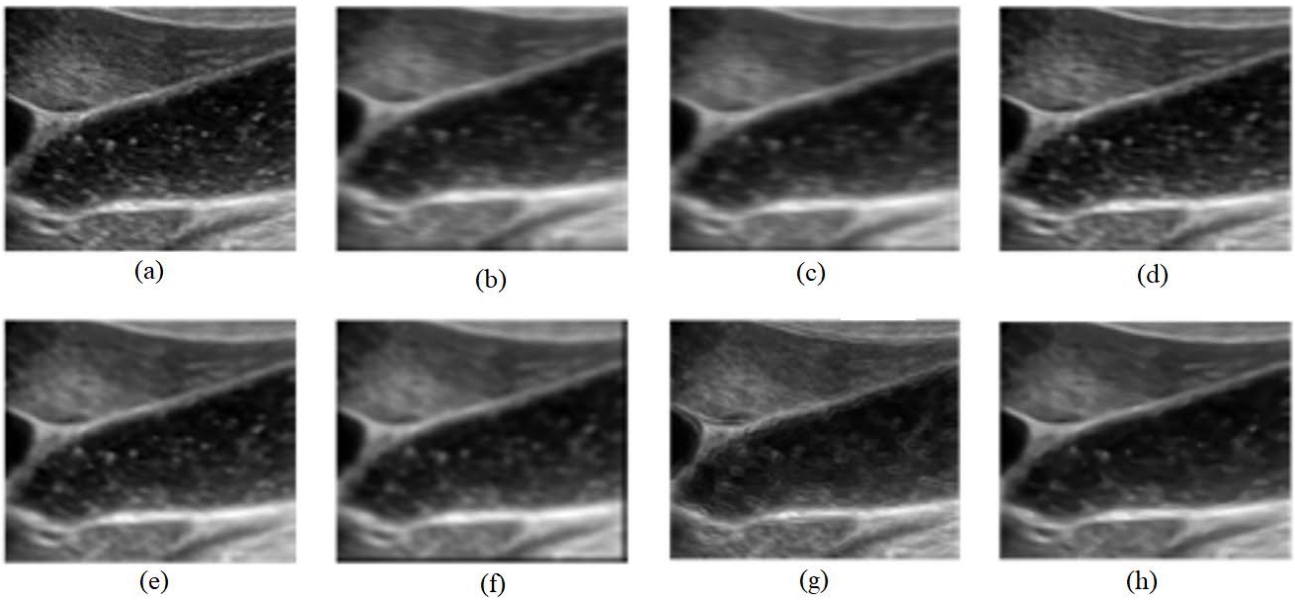

Fig. 5. Real gallbladder visual results: (a) – speckle noisy, (b) – frequency 8×8, 4, (c) –Schur-frequency 8×8, 4, (d) – Schur-regular 8×8, 4, (e) – Frost, (f) – Lee, (g) – PNLM, and (h) – TVF

This attracting result leads to dropping the Schur decomposition from the despeckling procedure and hence reducing the complexity of the despeckling algorithm. Table 1 lists the computational complexities of the different algorithms. The complexities of Frequency, Schur-frequency and Schur-regular can be reduced by half if the image is despeckled in the lateral and axial directions separately. Since the covariance matrix could be reduced in either direction, the resulting complexity for Schur-frequency and Schur-regular schemes could be $O\left(N^{3/2}\right)$ and for Frequency scheme $O\left([N/logN]^{1/2}\right)$. Obviously, the proposed frequency technique is the most attractive computational wise.

Figure 3 presents the comparative analysis of the lateral and axial profiles taken from the middle of the image of Fig. 2 that corresponds to Tab. 2. The proposed techniques show the best approximation to the noise-free image profiles in both lateral and axial directions. The benchmark schemes such as Schur-regular and TVF tend to show loose closeness to the true profiles. Frost and Lee performance is accompanied by ripples. The ripples that tend to be abrupt and spiky are clear in the PNLM performance. Among all, the proposed frequency technique

Table 4. Numerical results of real data

	Frequency			Schur-frequency			Schur-regular		
Block	4×4	8×8	8×8	4×4	8×8	8×8	4×4 4	8×8	8×8
Vectors	2	1	2	2	1	2	2	1	2
α	0.0542	0.1031	0.0968	0.0553	0.1031	0.0969	0.0523	0.1031	0.0928
β	0.1837	0.1676	0.2975	0.1818	0.1696	0.3020	0.1741	0.1674	0.2813
CNR	0.2304	0.2164	0.2147	0.2324	0.2155	0.2152	0.2291	0.2184	0.1841
SNR	13.2534	18.1667	20.1968	13.4043	18.1290	20.4012	12.4835	17.9838	20.5857
PSNR	22.0813	26.4122	27.6068	22.2195	26.4288	27.8330	21.3849	26.3517	27.2533
FSIM	0.8408	0.9213	0.9304	0.8455	0.9219	0.9319	0.8124	0.9227	0.9347

looks like the one that provided the closest fit to the noise free profiles.

5.2 Real ultrasound images

Real images of abdomen, gallbladder, lymph node and tumor are downloaded from [26] and cropped to the size of 256×256 as shown in Fig. 4(a), Fig. 5(a), Fig. 6(a) and Fig. 7(a), respectively. Since assessing measures are limited in case of real data due to the absence of the original image, the resolution parameter and the CR are the parameters that could be used for real data. By comparing the data in Tab. 2 with Tab. 3 for the block size 8×8 with 4 vectors and the block size 8×8 with two vectors, we can notice that the block size 8×8 with four vectors has provided a higher CR (the higher value indicates better contrast to noise ratio) and a lower value of α (the lower value indicates better resolution). Therefore, the choice of block size 8×8 with four vectors for real data will also implicitly indicate that the corresponding assessing measures (β, SNR, $PSNR$, $FSIM$) would be higher than those of benchmark schemes mainly, Frost, Lee, PNLM and TVF.

While the proposed schemes of Frequency and Schur-frequency and the benchmark scheme of Schur-regular are used with block size 8×8 with four vectors, the rest of benchmarking schemes of Frost, Lee, PNLM and TVF are found to be achieving better despeckling results with the same parameters listed in Tab. 1. The numerical outcomes are listed in Tab. 4, pertaining to ultrasound images of abdomen, gallbladder, lymph node and tumor.

Based on Tab. 4, it is obvious that the numerical assessment through α and CR solely, in the absence of other assessing measures, can be misleading. This is the case especially as α and CR for the proposed schemes are found outperforming those of the benchmark schemes for certain images, and are found underperforming by the benchmark schemes for other images. A quick example on this numerical variation can be seenin Tab. 2 for PNLM. PNLM in Tab. 2 has achieved the best resolution among all schemes with a value of (0.0390), and has achieved the best CR among all schemes as well with a value of (0.2454). However, with careful investigation of the numerical performance of PNLM and by looking at the other assessing measures, we can notice, and within the same Tab. 2, that PNLM has achieved a very poor performance compared to the proposed schemes in terms of β, SNR, $PSNR$ and $FSIM$.

As a result, visual assessment plays an important role in assessing the quality of the despeckled images. Satisfying visual results can be seen in Fig. 4(b) and (c) for frequency and Schur-frequency respectively, when applied to the speckle noisy abdomen in Fig. 4(a). Similar satisfying visual results are shown in the same respective in Fig. 5(b) and (c) for the speckle noisy gallbladder of Fig. 5(a). Fig. 6(b) and (c), as well as Fig. 7(b) and (c) reflect the same satisfying visual results for the speckle noisy lymph node and tumor displayed in Fig. 6(a) and in Fig. 7(a), respectively. PNLM continued to show artifacts as clear in image (g) in Fig. 4 through 7. Those artifacts are seen as abrupt spikes in Fig. 3 (in the profiles of the simulated experiment). In comparison with the proposed approaches, Frost and Lee are found inefficient in suppressing speckle noise as shown in images (e) and (f), respectively in Fig. 4 through 7.

Schur-regular and with the same despeckling parameters as the proposed schemes is not as efficient in suppressing speckle noise as can be seen in images (d) in Fig. 4 through 7. The drawback of the TVF is its trend to preserve speckle noise clusters. Although this drawback exists in image (h) in Fig. 4 through 7, it is quite apparent in Fig. 4(h) and Fig. 6(h).

6 Conclusion

This paper presents the despeckling of ultrasound images in the frequency domain. The covariance matrix obtained for each block is subjected to two proposed techniques; Frequency and Schur-Frequency. In either technique the covariance matrix is transformed to the frequency domain. In the case of the Frequency technique, the orthonormal vectors are taken directly from the Fourier transformed covariance matrix to form the projection matrix; whereas, in the case of the Schur-Frequency, the Fourier transformed covariance matrix is subjected to Schur decomposition. Orthonormal vectors are then

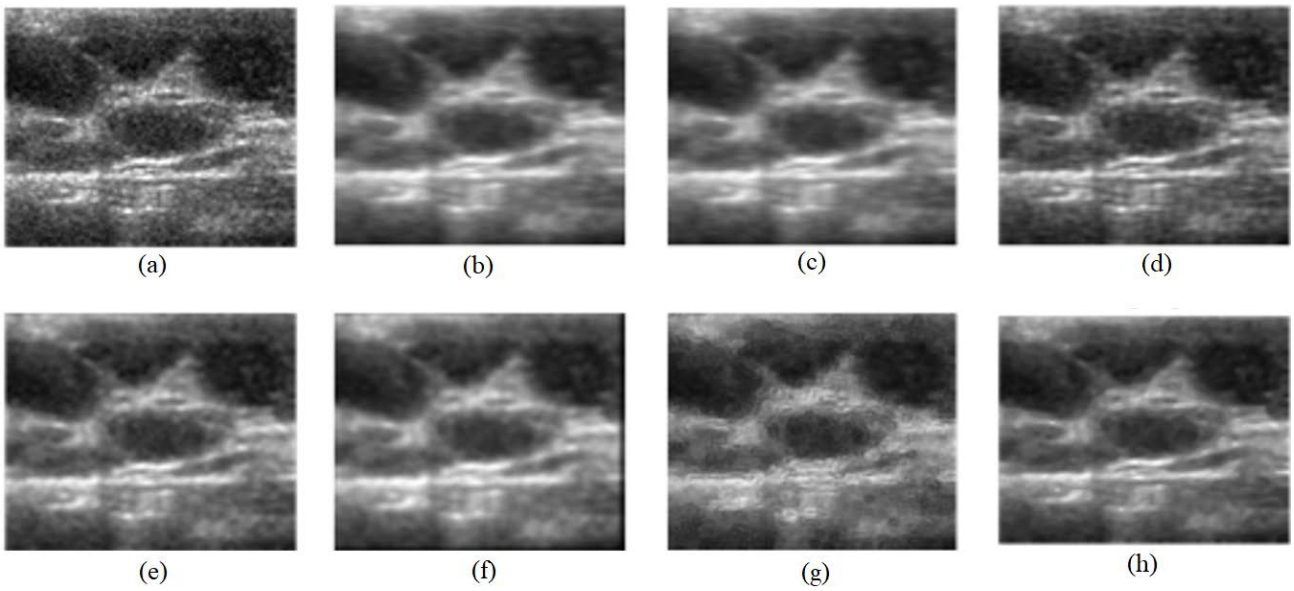

Fig. 6. Real lymph nodes visual results: (a) – speckle noisy, (b) – frequency 8×8, 4, (c) – Schur-frequency 8×8, 4, (d) – Schur-Regular $8 \times 8, 4$, (e) - Frost, (f) – Lee, (g) – PNLM and (h), TVF

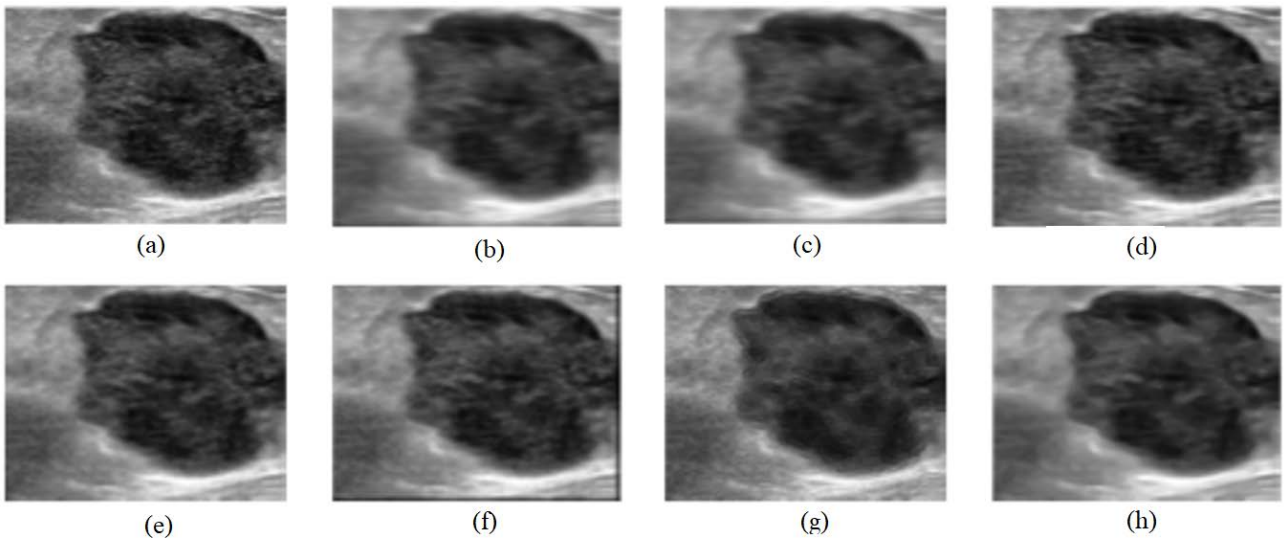

Fig. 7. Real tumor visual results: (a) – speckle noisyk, (b) – frequency $8 \times 8, 4$, (c) – Schur-frequency $8 \times 8, 4$, (d) – Schur-regular $8 \times 8, 4$, (e) - Frost, (g) – Lee, PNLM, and (h) – TVF

obtained from the Schur decomposition to form the projection matrix.

The main advantages of despeckling in the frequency domain over despeckling in the spatial domain include better suppression of speckle noise, avoiding image oversmoothing and reducing the computational complexity. The projection matrix formed from Schur decomposition in the frequency domain, called in this paper as Schur-Frequency, is found more efficient in suppressing speckle noise than the projection matrix formed from Schur decomposition in the spatial domain, called in this paper as Schur-Regular. The Schur-Frequency approach is found outperforming benchmark schemes such as Frost, Lee, PNLM and TVF. Moreover, the projection matrix formed directly from the Fourier transformed covariance matrix is found as efficient as the projection matrix formed within the Schur-Frequency approach in suppressing speckle noise.

A dyadic block size of 8×8 with four vectors is found suitable for a dyadic size of 256×256 image in treating the speckle noise. However, Schur-Regular performance is highly improved if a block size of 8×8 and two vectors

is used. This improvement is always found to be on the account of CR and the computational cost, especially when compared with the proposed Frequency approach.

References

[1] H. Yu, M. Ding, and X. Zhang, "PCANet based non-local means method for speckle noise removal in ultrasound images", *PLoS One*, vol. 13, no. 10, 2018. https: // doi.org/10.1371/journal.pone. 0205390.

[2] J. F. Al-Asad, M. O. Butt, and A. H. Khan, "Spectral Decomposition By Schur for Medical Ultrasound Image Denoising", *IEEE - International Symposium on Advanced Electrical and Communication Technologies*, 2019, https: //ieeexplore.ieee.org/ document /9069688.

[3] A. Piurica, W. Philips, I. Lemahieu, and M. Acheroy, "A versatile wavelet domain noise filtration technique for medical imaging", *IEEE Trans. Med. Imaging*, vol. 22, no. 3, pp. 323331, 2003, https://doi.org/10.1109/tmi.2003.809588.

[4] F. Baselice, "Ultrasound Image Despeckling Based on Statistical Similarity", *Ultrasound in Medicine &. Biology.*, vol. 43, no. 9, pp. 20652078, 2017, https://doi.org/10.1016/j.ultrasmedbio. 2017 .05.006.

[5] V. S. Frost, J. A. Stiles, K. S. Shanmugan, and J. C. Holtzman, "A Model for Radar Images and Its Application to Adaptive Digital Filtering of Multiplicative Noise", *IEEE Trans. Pattern Anal. Mach. Intell.*, vol. PAMI-4, no. 2, pp. 157-166, 1982. https: // doi.org/10.1109/tpami.1982.4767223.

[6] D. T. Kuan, A. A. Sawchuk, T. C. Strand, and P. Chavel, "Adaptive Noise Smoothing Filter For Images With Signal-Dependent Noise", *IEEE Trans. Pattern Anal. Mach. Intell.*, vol. PAMI-7, no. 2, pp. 165-177, 1985, https: //doi.org/10.1109/ tpami. 1985.47 67641.

[7] J.-S. Lee, "Digital Image Enhancement and Noise Filtering by Use of Local Statistics", *IEEE Trans. Pattern Anal. Mach. Intell.*, vol. PAMI-2, no. 2, pp. 165-168, 1980, https://doi.org/10.1109/ tpami.1980.4766994.

[8] Yu Yongjian and S. T. Acton, "Speckle reducing anisotropic diffusion", *IEEE Trans. Image Process.*, vol. 11, no. 11, pp. 1260-12 70, (2002). https:// doi.org/10.1109/tip.2002.804276.

[9] C. Tomasi and R. Manduchi, "Bilateral filtering for gray and color images", *Proceedings of the 1998 IEEE International Conference on Computer Vision*, pp. 839-846, 1998, https: // users.soe.ucsc.edu/ manduchi/Papers/ICCV98.pdf.

[10] A. Vishwa and S. Sharma, "Modified Method for Denoising the Ultrasound Images by Wavelet Thresholding", *Intell. Syst. Appl.*, vol. 4, no. 6, pp. 25-30, 2012, https:// doi.org/10.5815/ijisa .2012.06.03.

[11] Y. Farouj, J.-M. Freyermuth, L. Navarro, M. Clausel, and P. Delachartre, "Hyperbolic Wavelet-Fisz Denoising for a Model Arising in Ultrasound Imaging", *IEEE Trans. Comput. Imaging*, vol. 3, no. 1, pp. 1-10, 2017, https://doi.org/10.1109/tci. 2016.2625740.

[12] F. Zaki, Y. Wang, H. Su, X. Yuan, and X. Liu, "Noise adaptive wavelet thresholding for speckle noise removal in optical coherence tomography", *Biomed. Opt. Express*, vol. 8, no. 5, p. 2720, 2017, https:https://doi.org/10.2478/jee-2021-0032.org/10.1364 /boe.8.002720.

[13] Y. Zhan, M. Ding, L. Wu, and X. Zhang, "Non-local means method using weight refining for despeckling of ultrasound images", *Signal Processing*, vol. 103, pp. 201-213, 2014. https:// doi.org/10.1016/j.sigpro.2013.12.019.

[14] L. Zhu, C.-W. Fu, M. S. Brown, and P.-A. Heng, "A Non-Local Low-Rank Framework for Ultrasound Speckle Reduction", *The IEEE Conference on Computer Vision and Pattern Recognition (*, CVPR), pp. 5650-5658, 2017, https: // ieeexplore.ieee.org/ document/8099543.

[15] J. Yang, J. Fan, D. Ai, X. Wang, Y. Zheng, S. Tang, and Y. Wang, "Local statistics and non-local mean filter for speckle noise reduction in medical ultrasound image", *Neurocomputing*, vol. 195, pp. 88-95, 2016, https://doi.org/10.1016/j.neucom. 2015.05.140.

[16] C. A. N. Santos, D. L. N. Martins, and N. D. A. Mascarenhas, "Ultrasound Image Despeckling Using Stochastic Distance-Based BM3D", *IEEE Trans. Image Process.*, vol. 26, no. 6, pp. 2632-2643, 2017, https://doi.org/10.1109/tip.2017.2685339.

[17] Y. Wu, B. Tracey, P. Natarajan, and J. P. Noonan, "Probabilistic non-local means", *IEEE Signal Process. Lett.*, vol. 20, no. 8, pp. 763-766, 2013. https:// doi.org/10.1109/lsp.2013.2263135.

[18] J. F. Al-Asad and A. H. Khan, "QR based de-noising scheme for medical ultrasound images", *9 th IEEE-GCC Conference and Exhibition, GCCCE*,.

[19] A. H. Khan, J. F. Al-Asad, and G. Latif, "Speckle suppression in medical ultrasound images through Schur decomposition", IET *Image Process.*, vol. 12, no. 3, pp. 307-313, 2018, https:/ /doi.org/10.1049/iet-ipr.2017.0411.

[20] M. O. Butt, J. F. Al-Asad, A. H. Khan, and D. N. F. Awang Iskandar, "Ultrasound image denoising using orthogonal decomposition in frequency domain", *IEEE 9 th International Conference on System Engineering and Technology, ICSET 2019 - Proceeding*, pp. 349-353. 2019, https://ieeexplore.ieee.org /document/8906441.

[21] Y. Chen, M. Zhang, H.-M. Yan, Y.-J. Li, and K.-F. Yang, "A New Ultrasound Speckle Reduction Algorithm Based on Superpixel Segmentation and Detail Compensation", *Appl. Sci.*, vol. 9, no. 8, p. 1693, 2019, https://doi.org/10.3390/app9081693.

[22] Z. Hosseini and M. H. Bibalan, "Speckle noise reduction of ultrasound images based on neighbor pixels averaging", *25 th Iranian Conference on Biomedical Engineering and 3 rd International Iranian Conference on Biomedical Engineering*, ICBME 2018, https://ieeexplore.ieee.org/document/870 3576.

[23] O. V. Michailovich and A. Tannenbaum, "Despeckling of medical ultrasound images", *IEEE Trans. Ultrason. Ferroelectr. Freq. Control*, vol. 53, no. 1, pp. 64-78, 2006, https://ieeexplore.ieee.org/stamp/stamp.jsp?arnumber=1588392.

[24] J. A. Jensen, "Field: A Program for Simulating Ultrasound Systems", *Paper presented at the 10 th Nordic-Baltic Conference on Biomedical Imaging. Medical & Biological Engineering & Computing, Supplement 1, Part 1*, vol. 34, pp. 351-353, 1996. https: //field-ii.dk/documents/jaj_nbc_1996.pdf.

[25] A. Khvostikov, A. Krylov, J. Kamalov, and A. Megroyan, "Ultrasound despeckling by anisotropic diffusion and total variation methods for liver fibrosis diagnostics", *Signal Processing: Image Communication*, vol. 59 pp. 3-11, 2017, https: / /doi.org/10.1016/j.image.2017.09.005.

[26] J. Antony, "A Gallery of High-Resolution, Ultrasound, Color Doppler & 3D Images", *Ultrasound Image Gallery*, 2019, https://www.ultrasound-images.com.

Received 23 December 2020

Jawad F. Al-Asad is an Assistant Professor of Electrical Engineering at Prince Mohammad Bin Fahd University (PMU)/Saudi Arabia. He earned his PhD in Electrical Engineering from the University of Wisconsin-Milwaukee, USA in 2009. Prior to joining PMU, he was a senior professor at DeVry University-USA teaching in the biomedical, electrical and computer engineering technology majors. His research interests are in the field of biomedical signal and image processing and image reconstruction.

Hiren K. Mewada has obtained his M.Tech. and PhD degree from Sardar Vallbhbhai National Institute of Technology - Surat, Gujarat, India. Presently he is Assistant Research Professor at Prince Mohammad Bin Fahd University, Kingdom of

Saudi Arabia. His current areas of interest are computer vision, signal processing, machine learning and Embedded System design

Adil Humayun Khan is PhD candidate at (FCSIT), UNIMAS, Sarawak/Malaysia. He earned his Bachelors in Electrical Engineering (Telecom) from COMSATS university, Pakistan in 2008 and MS in Electrical Engineering from King Fahd University, Saudi Arabia in 2013 with specialization in Signal and Image Processing. His current research areas are adaptive signal processing, despeckling of ultrasound images and skin lesion detection.

Nidal Abu-Libdeh is an Assistant Professor of Physics and Chair of Core program at Prince Mohammad Bin Fahd University (PMU) in Saudi Arabia. He earned his Ph.D from McMaster University in Ontario, Canada in 2010. His research interests iclude Magnetic Ultrathin films, CFD. He is also interested in Interdisciplinary Research, where individuals with different backgrounds integrate their different perspectives and concepts to advance fundamental understanding.

Jamal Nayfeh is the Dean of the college of Engineering and a Professor of Mechanical Engineering at Prince Mohammad Bin Fahd University since 2009. Previously, he was the Associate Dean for Academics at the College of Engineering and Computer Science at the University of Central Florida. He received his PhD in Engineering Mechanics from Virginia Tech in 1990. Dr Nayfeh is a member of Tau Beta Pi Engineering Honor Society, American Society of Mechanical Engineers, Society of Petroleum Engineers and American Society for Engineering Education. His current fields of research/interests include CAD/CAM, Renewable Energy, Nondestructive Testing & Evaluation, Reliability & Maintenance Engineering, Artificial Intelligence and Engineering Education. Dr Nayfeh is a reviewer of a number of international journals. He is a Consultant to the US Navy, Lockheed Martin Missiles and Fire Control, Walt Disney World Ride and Show Engineering, Siemens Power Corporation, and US Corps of Engineers.